Heliyon 10 (2024) e32159

Contents lists available at ScienceDirect

Heliyon

journal homepage: www.cell.com/heliyon

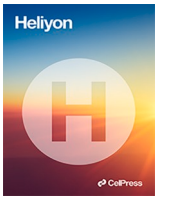

Research article

Bazi Bushen capsule attenuates cardiac systolic injury via SIRT3/SOD2 pathway in high-fat diet-fed ovariectomized mice

Xiaobin An [a,1], Wentao Xu [a,1], Xinyue Zhao [a], Haihui Chen [a], Jinan Yang [a], Yan Wu [a], Dongyang Wang [a], Wei Cheng [a], Hongrong Li [b,c], Lu Zeng [a], Jing Ma [a], Qin Wang [a], Xuqiao Wang [a], Yunlong Hou [b,c,**], Jing Ai [a,*]

[a] *Department of Pharmacology (The State-Province Key Laboratories of Biomedicine-Pharmaceutics of China), National Key Laboratory of Harbin Medical University, Harbin, Heilongjiang Province, 150086, China*

[b] *New Drug Evaluation Center, Shijiazhuang Yiling Pharmaceutical Co., Ltd., Shijiazhuang, Hebei Province, 050035, China*

[c] *National Key Laboratory for Innovation and Transformation of Luobing Theory, Shijiazhuang, Hebei Province, 050035, China*

ARTICLE INFO

Keywords:
Bazi Bushen capsule
Cardiac injury
Mitochondria
Reactive oxygen species
SIRT3/SOD2

ABSTRACT

Background: Bazi Bushen capsule (BZBS) is a Chinese herbal compound that is clinically used to treat fatigue and forgetfulness. However, it is still unclear whether and how BZBS affects heart function decline in menopausal women. This study aimed to examine the effect of BZBS on cardiac function in a high-fat diet-fed ovariectomy (HFD-fed OVX) mouse model and elucidate the underlying mechanism of this effect.

Methods: The experimental animals were divided into five groups: sham group, HFD-fed OVX group, and BZBS (0.7, 1.4, 2.8 g/kg) intervention groups. Senescence β-galactosidase staining and echocardiography were used to evaluate cardiac function. SwissTargetPrediction, KEGG and GO enrichment analyses were used to screen the underlying mechanism of BZBS. The morphological and functional changes in cardiac mitochondria and the underlying molecular mechanism were assessed by transmission electron microscopy, western blotting and biochemical assays. STRING database was used to analysis protein-protein interaction (PPI) network. Molecular docking studies were employed to predict the interactions of specific BZBS compounds with their protein targets.

Results: BZBS treatment ameliorated cardiac senescence and cardiac systole injury in HFD-fed OVX mice. GO and KEGG analyses revealed that the 530 targets of the 14 main components of BZBS were enriched mainly in the oxidative stress-associated pathway, which was confirmed by the finding that BZBS treatment prevented abnormal morphological changes and oxidative stress damage to cardiac mitochondria in HFD-fed OVX mice. Furthermore, the STRING database showed that the targets of BZBS were broadly related to the Sirtuins family. And BZBS upregulated the SIRT3 and elevated the activity of SOD2 in the hearts of HFD-fed OVX mice, which was also verified *in vitro*. Additionally, we revealed that imperatorin and osthole from the BZBS

* Corresponding author. Department of Pharmacology (The State-Province Key Laboratories of Biomedicine-Pharmaceutics of China), College of Pharmacy of Harbin Medical University, Harbin, Heilongjiang Province, 150086, China.

** Corresponding author. New Drug Evaluation Center, Shijiazhuang Yiling Pharmaceutical Co., Ltd., Shijiazhuang, Hebei Province, 050035, China.

E-mail addresses: houyunlonghrb@hotmail.com (Y. Hou), azhrbmu@126.com, aijing@ems.hrbmu.edu.cn (J. Ai).

[1] The first two authors contributed equally to this work.

https://doi.org/10.1016/j.heliyon.2024.e32159
Received 11 March 2024; Received in revised form 25 May 2024; Accepted 29 May 2024
Available online 31 May 2024

upregulated the expression of SIRT3 by directly docking with the transcription factors HDAC1, HDAC2, and BRD4, which regulate the expression of SIRT3.
Conclusion: This research shows that the antioxidative effect and cardioprotective role of BZBS on HFD-fed OVX mice involves an increase in the activity of the SIRT3/SOD2 pathway, and the imperatorin and osthole of BZBS may play central roles in this process.

Abbreviations

ATP	Adenosine triphosphate
BRD4	Bromodomain-containing protein 4
BZBS	Bazi Bushen capsule
HDAC1	Histone deacetylase 1
HDAC2	Histone deacetylase 2
HFD	High-fat diet
IVSd	Interventricular septal depth
IVSs	Interventricular septal thickness
LVEDV	Left ventricular end-diastolic volume
IVSd	Interventricular septal depth
IVSs	Interventricular septal thickness
LVEDV	Left ventricular end-diastolic volume
LVEF	Left ventricular ejection fraction
LVESV	Left ventricular end-systolic volume
LVFS	Left ventricular fraction shortening
LVIDd	Left ventricular end-diastolic diameter
LVPWDd	Left ventricular end-diastolic posterior wall thickness
LVPWs	Left ventricular posterior wall thickness
MDA	Malondialdehyde
OXPHOS	Oxidative phosphorylation
OVX	Ovariectomy
PPI	Protein-protein interaction
ROS	Reactive oxygen species
SIRTs	Sirtuins
SOD	Superoxide dismutase
TC	Total cholesterol
TCM	Traditional Chinese medicine
TG	Triglyceride

1. Introduction

The hallmark of female aging is a sharp decrease in estrogen levels during menopause, which increases susceptibility to cardiovascular disease and sudden cardiac death in women [1,2]. The key to healthy aging is preventing and mitigating age-related diseases. In the clinic, cardiovascular disease has emerged as the primary cause of mortality in menopausal women [3]. On the other hand, unhealthy dietary habits, such as a high-fat diet (HFD), are considered high risk factors for accelerating the aging process [4,5] and increasing cardiac dysfunction in postmenopausal women more than in men [6,7]. This phenomenon was further verified in animal experiments. A HFD for 12 weeks accelerated cardiac impairment and bone senescence in ovariectomized (OVX) mice [8,9]. These findings suggest that aging women with unhealthy HFD habits are more susceptible to developing a cardiac aging phenotype and an increased risk of cardiac dysfunction and even sudden cardiac death. Furthermore, the World Obesity Atlas 2023 Report reported that the number of obese women worldwide reached 466 million in 2020, and this figure will increase to 855 million in 2035 (https://data.worldobesity.org/publications). Therefore, there is an urgent need to develop an effective intervention strategy to prevent or treat cardiac dysfunction in obese women with estrogen deficiency who are suffering from either menopause or ovariectomy.

Bazi Bushen capsule (BZBS) is a Chinese compound medicine which contains 16 kinds of traditional Chinese herbs (Table S1) [10]. In the clinic, BZBS is used to relieve several aging-related symptoms, such as fatigue and forgetfulness [11]. Animal studies have shown that BZBS mitigates epigenetic aging and extends the health span in naturally aging mice [12] and rescues sperm morphological remodeling and regeneration in D-galactose- and $NaNO_2$-induced aging mouse models via the SIRT6-mediated P53 and NF-κB pathways [13]. More importantly, BZBS can improve a series of menopause related-symptoms, such as increasing serum estrogen and lipid metabolism levels in HFD-fed OVX mice, alleviating atherosclerosis in HFD-fed OVX mice through GPER1-dependent

anti-inflammatory and anti-apoptotic effects, and effectively increasing bone density in OVX rats [14–16]. However, whether BZBS has potential for preventing cardiac injury in HFD-fed OVX mice needs to be further verified.

Mitochondrial oxidative stress is a common hallmark of senescence in all tissues of the body [17]. The sirtuins (SIRTs) family is reportedly involved in the development of cardiovascular disease [18] and plays an important role in the mitochondrial oxidative phosphorylation (OXPHOS) process [19]. Downregulation of SIRT2 by microRNA-140 exacerbates doxorubicin-induced cardiotoxicity by promoting myocardial oxidative stress [20]. Moreover, SIRT3 deficiency increases ROS accumulation and exacerbates diabetic cardiomyopathy [21]. The heart is the most energy-demanding organ and is extremely sensitive to mitochondrial oxidative stress [22]. Previous studies have demonstrated that either estrogen deficiency or a HFD could result in mitochondrial metabolism disorders [23, 24]. A HFD was reported to accelerate cardiac dysfunction in mice induced by estrogen deficiency by increasing mitochondrial ROS production [8]. However, whether BZBS can rescue the cardiac dysfunction of estrogen-deficient mice induced by a combination of HFD through relieving mitochondrial oxidative damage through SIRT-related pathways is unknown. In this study, we demonstrated that BZBS reversed mitochondrial oxidative damage and systolic injury in HFD-fed OVX mice, and the mechanism involves an increase in the activity of the SIRT3/SOD2 pathway. Furthermore, the bioactive compounds that play central roles may be imperatorin and osthole in BZBS.

2. Materials and methods

2.1. Chemicals and reagents

BZBS capsules were obtained from Yiling Pharmaceutical Co., Ltd. (Lot: 2104001, Shijiazhuang, China). The BZBS suspension was dissolved in 0.5 % sodium carboxymethylcellulose (CMC-NA, Cat # 419281, USA, Sigma), and the suspension was administered to OVX mice by intragastric administration.

The BZBS freeze-dried powder was prepared in a lyophilizer. Briefly, after dissolving in 50 % dimethyl sulfoxide aqueous solution and centrifuging, the BZBS supernatant was frozen at −70 °C. After freezing for 24 h, the supernatant was freeze-dried in a lyophilizer.

A high-fat diet (Cat #H10060) was purchased from Beijing Huafukang Biotechnology Co., Ltd. (Beijing, China). The compositions of the HFD were shown in Table S2.

2.2. Animals

C57BL/6 mice (female, 18–22 g, 8 weeks old) were obtained from Liaoning Changsheng Biotechnology Co., Ltd. (Benxi, China). Animals were housed in an animal feeding room with controlled humidity (55 ± 5 %) and temperature (23 ± 1 °C) conditions. The mice were maintained on a 12 h dark/light artificial cycle with water and food available *ad libitum*. All animal procedures were approved by the Institutional Animal Care and Use Committee at Harbin Medical University (No. IRB3000722) and the Institute of Laboratory Animal Science of China (A5655-01). All procedures conformed to Directive 2010/63/EU of the European Parliament and the ARRIVE guidelines.

Ovariectomy (OVX) surgery was performed as previously described [25,26]. Briefly, after the mice were anesthetized with sodium pentobarbital (100 mg/kg, i. p.), a 1 cm longitudinal incision was made in the back of each mouse. After both ovaries were ligated, the mice were placed in an incubator. In the sham group, the ovaries were not removed; instead, adipose tissue similar in the volume to the ovary was removed to mimic the trauma of an ovariectomy. One week after postoperative recovery, the OVX mice were randomly divided into five groups, as shown in Table S3. The OVX mice were intragastric (i.g.) administration with vehicle (0.5 % CMC-Na) or BZBS together with a high-fat diet (HFD) for 12 weeks. The dosages of BZBS were 0.7 g/kg/day, 1.4 g/kg/day and 2.8 g/kg/day.

2.3. Echocardiography

The echocardiographic examination was performed as previously described [25,27]. Mice were anesthetized and fixed in a supine position on a constant temperature heating fixing plate. Hair removal cream was applied to the chest to remove the fur. The coupling agent was applied to the region from the neck to the sternal lobule. Two-dimensional ultrasound images of the left ventricle were obtained in M-mode. The left ventricular end-systolic volume (LVESV), left ventricular internal dimension (LVIDs), interventricular septal thickness (IVSs), left ventricular posterior wall thickness (LVPWs), left ventricular end-diastolic volume (LVEDV), left ventricular end-diastolic diameter (LVIDd), and left ventricular end-diastolic posterior wall thickness (LVPWDd) of the mice were measured in B-mode. Then, the left ventricular ejection fraction (LVEF) and left ventricular fraction shortening (LVFS) were calculated.

2.4. Transmission electron microscopy

The samples were processed as follows: left ventricular samples were added to 2.5 % glutaraldehyde fixative solution for 3 days at 4 °C; after three washes with PBS, 1 % osmium acid fixative solution was added, and the samples were fixed at 4 °C for 2–3 h; the samples were dehydrated with gradient acetone; next, the samples were soaked in resin at room temperature overnight; then, at three different polymerization temperatures, 37 °C, 45 °C, one day, and 60 °C, one day; finally, the samples were sliced to a thickness of 70 nm; stained with uranium dioxygen acetate for 15 min; and stained with lead citrate for 10 min [28]. The ultrastructure and morphological changes of the cardiac mitochondria were observed using transmission electron microscopy (JEM-1220, JEOL Ltd., Japan) after drying, and the mitochondrial area was measured by ImageJ software.

2.5. Cell culture

H9C2 cells were purchased from ATCC (CRL-1446). H9C2 cells were cultured cultured in DMEM (Cat # 11965092, Invitrogen, USA) supplemented with 0.1 % P/S (Cat #G1236, Solarbio, China) and 10 % FBS (Cat # SV30208.03, HyClone, USA) in a 37 °C incubator with humidified air and 5 % CO2. The experiments were performed after 2–4 generations of cell transmission. Then, 50 nM SIRT3 siRNA (Ribobio, China), 50 nM SIRT3 siRNA + 400 μg/mL BZBS, or NC siRNA was transfected into H9C2 cells with X-treme GENE siRNA transfection reagent (Roche, Switzerland) according to the manufacturer's instructions. Forty-eight hours after transfection, the cells were collected for protein purification.

2.6. Cell viability assay

MTT cell viability assay kit (Cat #C0009S, Beyotime, China) was used for the detection of cell proliferation and cytotoxicity. H9C2 cells were seeded into 96-well plates at a density of 1×10^5 cells per well. Twenty-four hours after seeding, the culture medium was replaced with serum-free endothelial special culture medium supplemented with 50 nM SIRT3 siRNA, and different concentrations of BZBS were added to each well (50, 100, 200, 400, 800, 1000, and 1600 μg/mL). After 48 h, 10 μL of the MTT stock solution was added to each well and incubated at 37 °C for 4 h 100 μL of formazan solution was added to each well, the absorbance was measured at 570 nm after all the solution was dissolved, and the survival rate was statistically analyzed.

2.7. Quantitative real-time PCR

Total RNA was extracted from cells using TRIzol (Cat # 15596026, Invitrogen, USA) according to the manufacturer's protocol. SIRT3 mRNA was quantified with a ReverTra AceqPCR RT Kit (Cat # FSQ-201, Toboyo Co., Japan) and TaqMan Gene Expression Master Mix (Cat # 4369016, Applied Biosystems, Carlsbad, USA). The following qPCR primer sequences were used: SIRT3: forward: 5′-ACAGCTACATGCACGGTCTG -3'; reverse: 5′- ACACAATGTCGGGTTTCACA -3'; Gapdh: forward: 5′- TGTGTCCGTCGTGGATCTGA -3'; reverse: 5′- TTGCTGTTGAAGTCGCAGGAG -3'. SIRT3 mRNA expression was normalized to that of the internal control using the δ–δ CT method.

2.8. Adenosine triphosphate (ATP) assay

ATP levels were measured by an ATP assay kit (Cat #S0026B, Beyotime, China). Protein supernatant was collected from cells or tissues. Protein concentrations were determined by the BCA protein assay kit (Cat #P0010, Beyotime, China) for subsequent calculation of ATP content within tissues or cells by protein concentrations. Then, 100 μL of ATP assay working solution was added to the test tube. After incubation at room temperature for 3–5 min, 20 μL of sample or standard was added to the wells, and after at least 2-sec intervals, the relative luciferase activity (RLU) was determined. Finally, the concentration of ATP was calculated according to the standard curve.

2.9. Malondialdehyde (MDA) assay

The lipid oxidation levels were measured by an MDA assay kit (Cat #S0131S, Beyotime, China). After the tissues or cells were fully lysed, the protein supernatant was collected. Protein concentrations were determined by a BCA protein assay kit for subsequent calculation of the MDA content within tissues or cells according to protein concentrations. After the reaction system was prepared, it was heated at 100 °C for 15 min, cooled in a water bath to room temperature, and centrifuged at room temperature at 1000 g for 10 min. Subsequently, 200 μL of supernatant was added to the 96-well plate, and the absorbance was measured at 532 nm using a microplate reader. The molar concentration of the obtained MDA was calculated according to the standard curve, and the MDA content/per protein weight was calculated.

2.10. Isolation of adult mouse cardiomyocytes

Adult mouse cardiomyocytes were isolated as described in previous studies [29,30]. The heart was removed quickly after anesthesia and fixed to a constant flow of Langendorff apparatus through the aortic cannula. Tyrode's solution contained 1 mg/mL Type II collagenase powder, 0.02 mg/mL protease, and 1 mg/mL BSA, which was used to digest the heart by infusion. After the tissue softened, the left ventricle was gently cut into small pieces and stirred to isolate cardiomyocytes in Tyrode's solution supplemented with 200 μM CaCl2 and 1 % bovine serum albumin. All solutions were gassed with 95 % O_2 and 5 % CO_2 and maintained at 37 ± 0.5 °C.

2.11. Reactive oxygen species (ROS) assay

Intracellular reactive oxygen species levels were measured with a reactive oxygen species assay kit (Cat #S00052, Beyotime, China). The fluorescent label DCFH-DA was diluted with serum-free medium at a ratio of 1:1000. After isolation, adult mouse cardiomyocytes were suspended in serum-free medium. For adherent cells, the original medium in the 24-well plate was discarded, and 200 μL of serum-free medium was added to each well. The cells were incubated for 20 min at 37 °C. After incubation, the cells were washed with serum-free medium three times, and the level of reactive oxygen species was detected by flow cytometry (Beckman

Coulter Biotechnology, China). The results were analyzed using CytExpert software (Beckman Coulter Biotechnology, China).

2.12. Superoxide dismutase (SOD) assay

SOD activity was measured by an SOD assay kit (Cat #S01103, Beyotime, China). After lysis and homogenization, the tissues or cells were centrifuged at 12,000 g at 4 °C for 3–5 min. The supernatant was collected, and the protein concentration was determined with a BCA protein assay kit. To detect the mitochondrial SOD (Mn-SOD or SOD2) content, a Cu/Zn-SOD inhibitor was used. After Cu/Zn-SOD inhibition was performed, the samples and various other solutions were added to a 96-well plate according to the instructions. After incubation at 37 °C for 30 min, the absorbance was measured at 450 nm. The Mn-SOD content was calculated from the absorbance.

2.13. Senescence β-galactosidase staining kit

The heart was fixed with 4 % paraformaldehyde overnight at 4 °C and dehydrated with 30 % sucrose until it sank to the bottom of the fluid. Then, the heart was cut into 5 μm thick slices. A senescence β-galactosidase staining kit (Cat #C0602, Beyotime, China) was used to stain senescent cells according to the manufacturer's instructions. Images were taken using an LSM800 710 confocal microscope (Zeiss, Germany).

2.14. Western blot

Total protein was extracted from the left ventricle or H9C2 cells. A BCA protein assay kit was used to detect protein concentrations. The protein samples were loaded on a 10 % polyacrylamide gel for electrophoresis, transferred onto nitrocellulose membranes and incubated with the following primary antibodies: anti-SIRT1 (1:800, Cat # A11267, ABclonal, China), anti-SIRT2 (1:600, Cat # A0273, ABclonal, China), anti-SIRT3 (1:1,000, Cat # 5490S, Cell Signaling Technology, USA), anti-SIRT4 (1:600, Cat # A7585, ABclonal, China), anti-SIRT5 (1:600, Cat # A23083, ABclonal, China), anti-SIRT6 (1:600, Cat # A7416, ABclonal, China), and anti-β-actin (1:20000, ABclonal, China). The membranes were incubated with fluorescent secondary antibodies (1:10000, LICOR Biosciences, USA) for 1 h, and the bands were visualized using an Odyssey Infrared Imaging System (LICOR Biosciences, USA). Image Studio 5.2.5 software (LICOR Biosciences, USA) was used to measure the band intensity. Protein expression was normalized to that of the internal control, β-actin.

2.15. Data mining for network pharmacology

We constructed BZBS compound-target and BZBS target-sirtulin family networks using Cystoscope software (version 3.9.1). The STRING 11.5 database (https://string-db.org/) was used to construct the BZBS target-sirtuin family interaction network. SwissTargetPrediction (http://swisstargetprediction.ch/) was used to predict the targets of 14 components in BZBS. hTFTarget (http://bioinfo.life.hust.edu.cn/hTFtarget) was used to identify transcription factors among the targets of BZBS compounds and transcription factors that can regulate SIRT3.

2.16. Bioinformatic analysis

Gene Ontology (GO) and Kyoto Encyclopedia of Genes and Genomes (KEGG) enrichment analyses were carried out using the R "clusterProfiler" and "ggplot 2" packages. A P value < 0.05 for both the GO and KEGG enrichment analyses was considered to indicate statistical significance. The sequencing data of estrogen deficiency and long-term high-fat diet-fed mice were obtained from the GEO database (GSE55936 and GSE150229).

2.17. Autodocking for virtual screening

The 14 compounds (Fig. S1 and Table S4) in BZBS were docked with the transcription factor SIRT3. The protein crystal structures of BRD4, HDAC1, and HDAC2 were downloaded from the AlphaFold Protein Structure Database (https://alphafold.com/). The 3D structures of the 14 compounds were downloaded from NCBI-PubChem (https://pubchem.ncbi.nlm.nih.gov/). Finally, the 3D conformers of protein receptors and small molecule ligands were used for molecular docking in AutoDock 1.5.7, and the docking position of the minimum free energy appeared in PyMOL 2.5.0.

2.18. Statistical analysis

All the data were analyzed and are presented as the mean ± standard errors (mean ± SEM). Comparisons among groups were performed by one-way analysis of variance (ANOVA). Post hoc analyses of significant main effects were performed using Tukey post hoc tests for further examination. Two-tailed Student's t tests were used for comparisons between two groups. A P value < 0.05 indicated statistical significance, and GraphPad Prism 8.0 software (La Jolla, USA) was used for all the graphs.

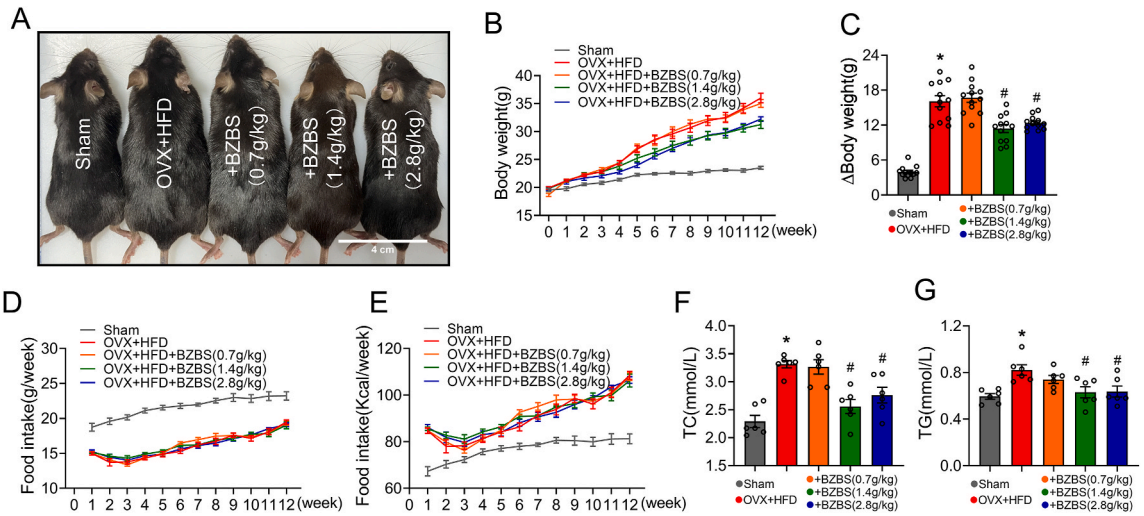

Fig. 1. Effects of BZBS on the diet and body weight of HFD-fed OVX mice. (A) Representative image showing 12-week-old normal-fed sham, HFD-fed OVX, and BZBS-treated HFD-fed OVX mice. Scale bar, 4 cm. (B) Body weight was monitored weekly for the sham, HFD-fed OVX, and BZBS-treated HFD-fed OVX mice. (C) Comparison of body weight gain at the 12th week in each group. n = 12 mice. (D) Food intake (g) was monitored weekly for the sham, HFD-fed OVX, and BZBS-treated HFD-fed OVX mice. (E) Food intake (Kcal) was monitored weekly. (F–G) Plasma TC (F) and TG (G) were detected for each group at the end of 12 weeks. n = 6 mice for each group, mean ± SEM, $^{*}P < 0.05$ *versus* the sham group, $^{\#}P < 0.05$ *versus* the OVX + HFD group.

3. Results

3.1. BZBS prevents HFD-induced obesity in OVX mice without changing food intake

First, we observed the effects of BZBS on food intake and body weight in HFD-fed OVX mice by daily gavage for 12 weeks. As shown in Fig. 1A–C, after a 12-week drug intervention, HFD-fed OVX mice displayed a markedly more obese phenotype than sham mice, which was prevented by daily gavage of BZBS at dosages of 1.4 and 2.8 g/kg. However, BZBS at a dose of 0.7 g/kg did not affect body weight in HFD-fed OVX mice (Fig. 1A–C). Although BZBS did not restore body weight (Fig. 1B), it significantly inhibited weight gain in HFD-fed OVX mice (Fig. 1C). Here, we found that the weekly food intake of HFD-fed OVX mice was significantly lower than that of sham mice (Fig. 1D), but caloric intake gradually increased (Fig. 1E). Interestingly, none of the doses of BZBS influenced the food or caloric intake of HFD-fed OVX mice (Fig. 1D and E). Furthermore, HFD-fed OVX mice showed abnormal serum lipid levels characterized by increased total cholesterol (TC) and triglyceride (TG) levels (Fig. 1F and G), suggesting that a successful mouse model was developed. BZBS restored the serum lipid levels of HFD-fed OVX mice to those of sham control mice (Fig. 1F and G). The above results suggest that BZBS has greater effects on weight and fat loss in mice that are estrogen deficient and fed a high-fat diet.

3.2. BZBS ameliorates cardiac systolic dysfunction in HFD-fed OVX mice

Next, to evaluate whether OVX mice fed a HFD for 12 weeks displayed a cardiac senescence phenotype, we performed a β-galactosidase staining experiment. Compared to that in sham mice, a positive β-galactosidase signal was markedly detected in myocardial tissue, which was successfully prevented by BZBS at doses of 1.4 and 2.8 g/kg but not 0.7 g/kg (Fig. 2A). These data suggest that BZBS has potential anti-myocardial senescence effects. We then evaluated cardiac function using echocardiography (Fig. 2B). The left ventricular ejection fraction (LVEF) and left ventricular fraction shortening (LVFS) are indices used to assess cardiac systolic ability. As shown in Fig. 2C and D, both the LVEF and LVFS decreased in HFD-fed OVX mice, and this decrease was reversed by treatment with BZBS at dosages of 1.4 g/kg/day and 2.8 g/kg/day. As a consequence of the decrease in the LVEF and LVFS, the left ventricular end-systolic volume (LVESV) was increased in HFD-fed OVX mice, and as expected, this change was distinctly reversed by the administration of BZBS (1.4 and 2.8 g/kg) (Fig. 2E). This finding confirmed that BZBS improved the reduction in cardiac systole in HFD-fed OVX mice. BZBS at a dose of 0.7 g/kg failed to block any of the decreases in cardiac systolic function. The left ventricular end-diastolic volume (LVEDV) and left ventricular end-diastolic diameter (LVIDd) can be used to evaluate cardiac diastolic ability. However, a HFD for 12 weeks did not affect the cardiac diastolic function of OVX mice, and BZBS had no effect (Fig. 2F and G). In addition, there were no differences in left ventricular posterior wall thickness (LVPWs), interventricular septal thickness (IVSs), left ventricular end-diastolic posterior wall thickness (LVPWDd), or interventricular septal depth (IVSd) among the groups (Fig. 2H–K). Taken together, these data verify that HFD-fed OVX mice exhibit systolic cardiac injury without changes in cardiac diastolic function and that BZBS prominently ameliorates this phenomenon.

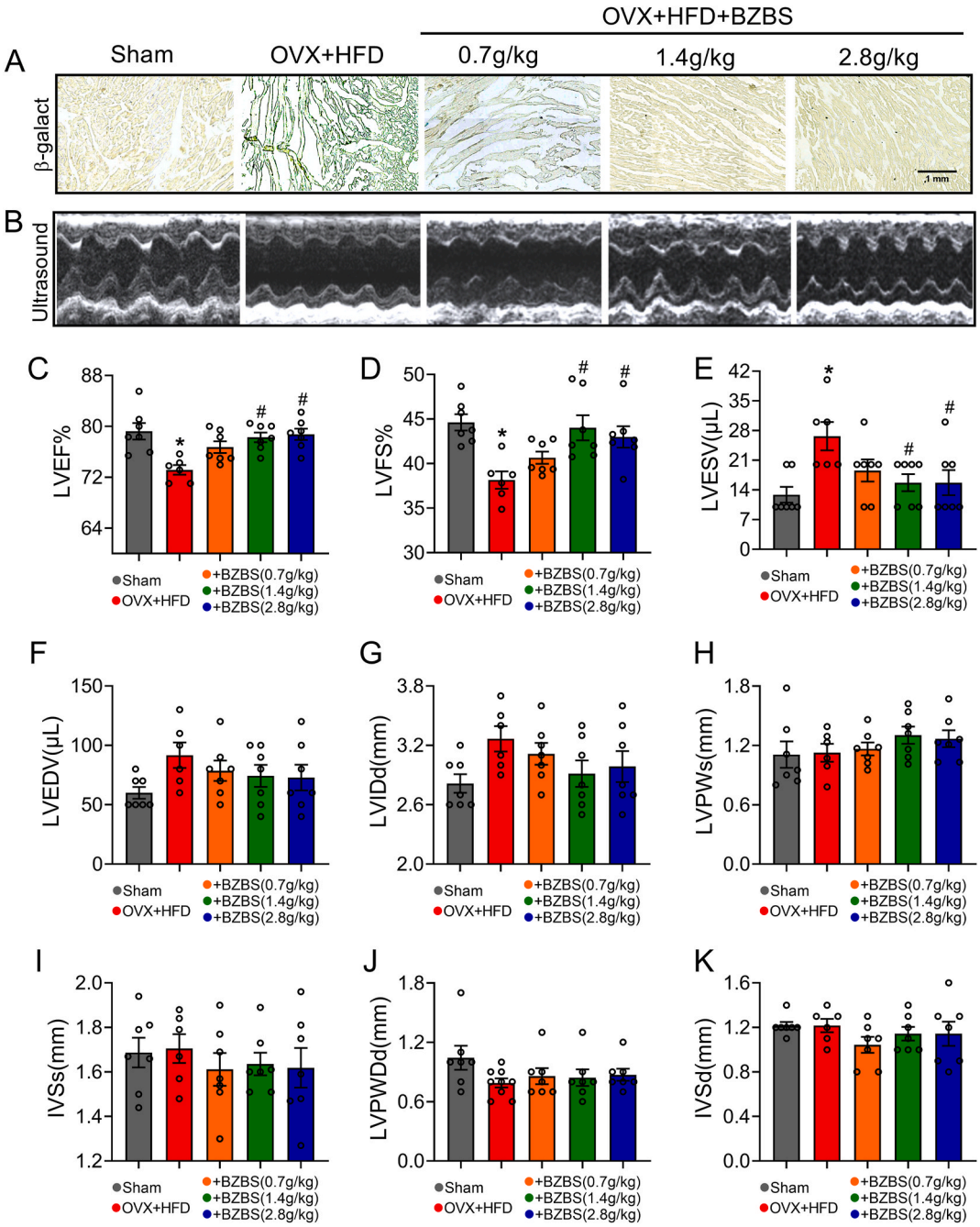

Fig. 2. Effects of BZBS on cardiac function in HFD-fed OVX mice. (A) Representative images of cardiac senescence stained with a β-galactosidase kit in each group. (B) M-mode echocardiograms of the left ventricle. (C–E) Effects of BZBS on the LVEF (C), LVFS (D), and LVESV (E) in HFD-fed OVX mice. (F–K) There were no differences in the LVEDV (F), LVIDd (G), LVPWs (H), IVSs (I), LVPWDd (J), or IVSd (K). n = 6–7 for each group, mean ± SEM, $^{*}P < 0.05$ *versus* the sham group, $^{\#}P < 0.05$ *versus* the OVX + HFD group.

3.3. BZBS alleviates cardiac mitochondrial impairment in HFD-fed OVX mice

A previous study reported that using ultra-performance liquid chromatography (UPLC/MS) analysis, there are 14 main components (Fig. S1 and Table S4) were found in BZBS capsule [31], suggesting that these components may be the material basis for the therapeutic effect of BZBS. To further explore the possible mechanisms underlying the protective effect of BZBS on HFD-fed OVX mice, we used Swiss Target prediction (STP) to predict the potential targets of the 14 components. We predicted 530 protein targets that interact with the 14 components (Fig. 3A–B). Interestingly, by performing KEGG analysis, we found that these predicted proteins were significantly

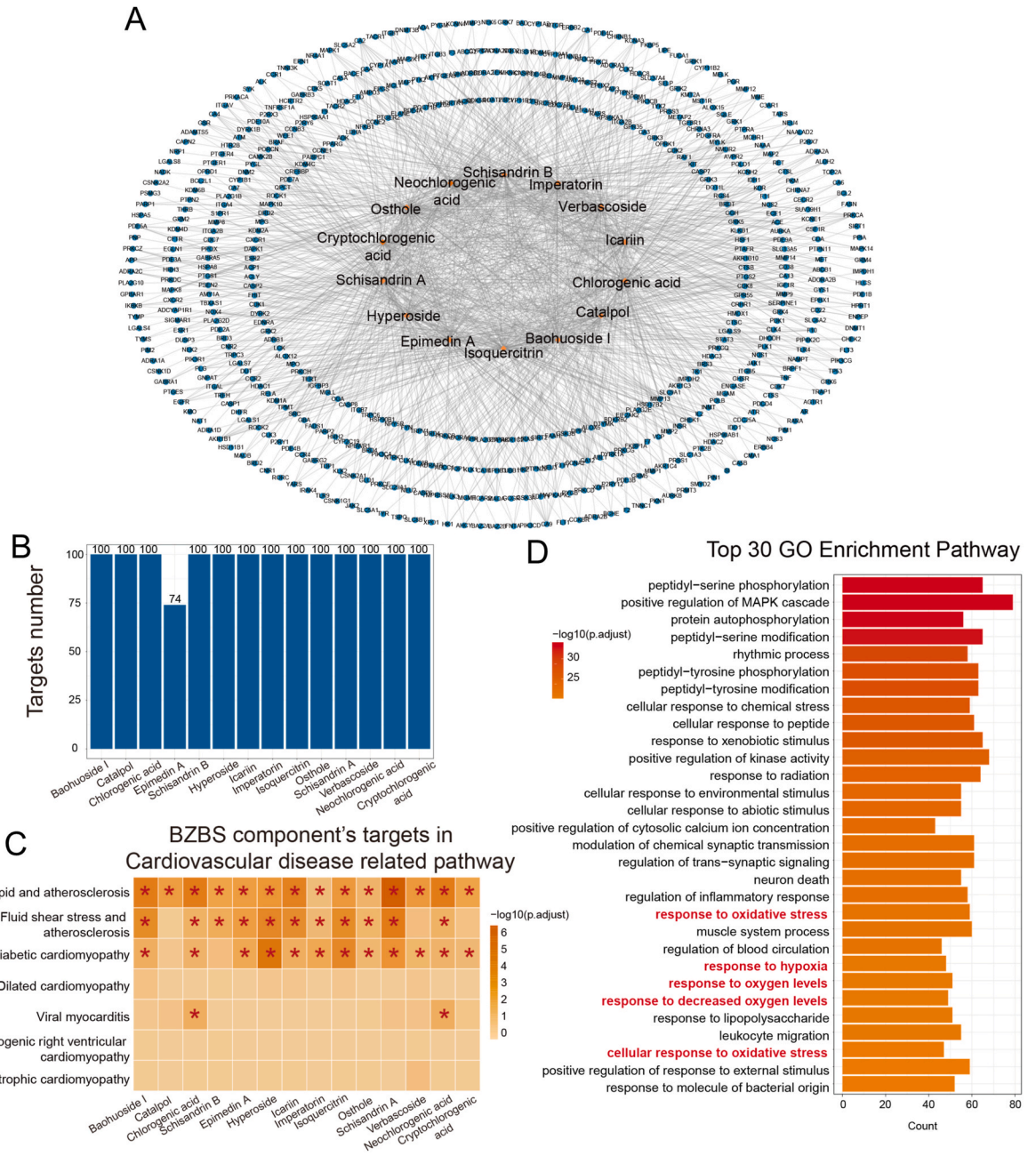

Fig. 3. Components in BZBS and their corresponding targets. (A) Network of 14 components of BZBS and their correlated targets. (B) The number of targets of 14 components in BZBS predicted by SwissTargetPrediction. (C) KEGG enrichment analysis of the targets of the 14 components of the cardiovascular disease pathway in BZBS. (D) Top 30 pathways of gene ontology (GO) enrichment analysis of target genes in components of BZBS. *$P < 0.05$.

correlated with cardiovascular disease-related pathways (Fig. 3C). On the other hand, GO enrichment analysis revealed that, within the top 30 pathways, 5 pathways were enriched in oxidative stress-related pathways involving response to oxidative stress, response to hypoxia, response to oxygen levels, response to decreased oxygen levels and cellular response to oxidative stress (Fig. 3D). These results show that the protective effects of BZBS on heart function in OVX mice fed a HFD might be associated with oxidative stress.

To biologically verify whether the effect of BZBS on impaired cardiac diastolic function in HFD-fed OVX mice involves antioxidant activity, we performed a series of studies. Using transmission electron microscopy (TEM), we found significantly more lipid droplets in the cardiomyocytes of HFD-fed OVX mice than in those of sham mice (Fig. 4A and B). In addition, we observed obvious structural remodeling of cardiac mitochondria in the cardiomyocytes of HFD-fed OVX mice, including abnormal mitochondrial ridges and

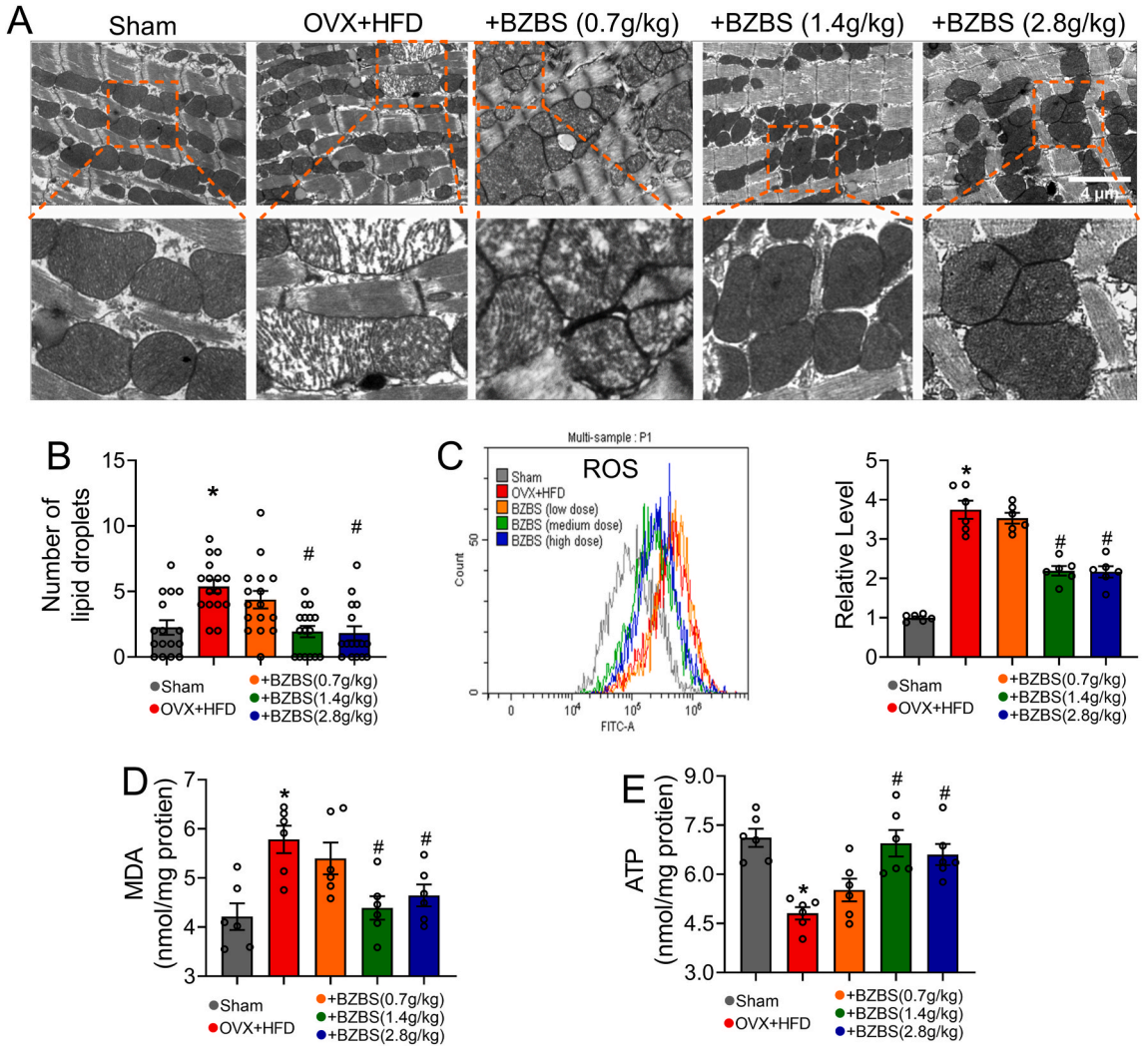

Fig. 4. Effects of BZBS on cardiac mitochondrial morphology and function in HFD-fed OVX mice. (A) Representative images of mitochondrial morphology in each group. Scale bar: 4 μm. (B) Number of lipid droplets in each group (n = 16 cells from 4 mice). (C) Representative histograms of the mean fluorescent intensity (MFI) for ROS in the sham, HFD-fed OVX, and BZBS-treated HFD-fed OVX mice. The MFI of ROS in all groups was quantified. (D–E) The MDA content (D) and ATP content (E) were detected in each group. n = 6 for each group, mean ± SEM, $^{*}P < 0.05$ *versus* the sham group, $^{\#}P < 0.05$ *versus* the OVX + HFD group.

increased vacuolation, which was not observed in the sham controls (Fig. 4A). As predicted, BZBS treatment (1.4 and 2.8 g/kg) markedly alleviated all these changes (Fig. 4A and B). It has been reported that excessive lipid droplets are associated with increased mitochondrial ROS levels [32]. Increased ROS can cause lipid peroxidation, which can lead to increased malondialdehyde (MDA) levels and reduced ATP production [33,34]. Here, we found that BZBS (1.4 and 2.8 g/kg) effectively blocked the increases in ROS (Fig. 4C) and MDA levels (Fig. 4D) and decreased ATP level (Fig. 4E) in the cardiomyocytes of HFD-fed OVX mice. BZBS at a dose of 0.7 g/kg failed to exert all of the above protective effects on cardiac mitochondria in HFD-fed OVX mice. These results demonstrate that the cardioprotective effect of BZBS on the HFD-fed OVX mouse model involves its antioxidative effect on stress.

3.4. The SIRT3/SOD2 pathway mediates the antioxidative effect of BZBS

The SIRTs family has been reported to play an important role in regulating ROS levels and maintaining mitochondrial homeostasis [35]. To elucidate whether the molecular mechanism of the cardioprotective effect of BZBS in HFD-fed OVX mice is associated with SIRTs, we performed protein-protein interaction (PPI) network analysis with the STRING database. Coincidentally, the corresponding targets of BZBS had a broad relationship with the SIRTs family (Fig. 5A). By analyzing the GSE55936 and GSE150229 datasets from the GEO database, which include heart-specific estrogen receptor knockout (KO mice, 18 weeks) and long-term high-fat diet (16 weeks) data, we found that the expression of SIRT3 and SIRT5 in the hearts of 18-week-old KO mice was significantly lower than that in the

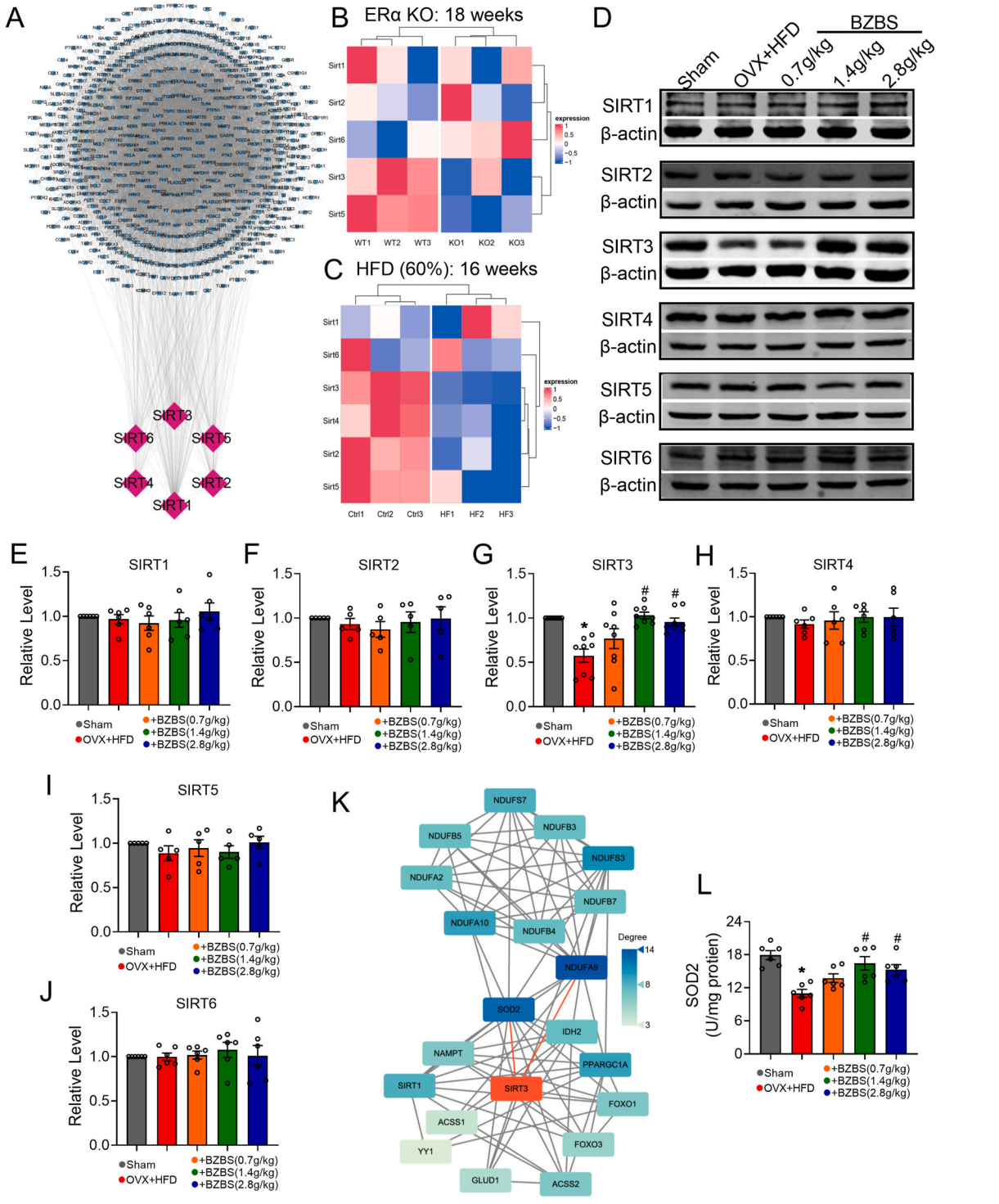

Fig. 5. BZBS regulated the SIRT3/SOD2 pathway in HFD-fed OVX mice. (A) Relationships between the SIRTs family and the corresponding targets of BZBS. (B) The expression of the cardiac SIRTs family in heart-specific estrogen receptor knockout mice. (n = 3). (C) The expression of the cardiac SIRTs family in HFD-fed mice. (n = 3). (D) Representative immunoblotting images of SIRTs and β-actin. (E–J) Cardiac SIRT1 (E), SIRT2 (F), SIRT3 (G), SIRT4 (H), SIRT5 (I), and SIRT6 (J) expression in each group. The cardiac SIRT3 protein level was significantly decreased in HFD-fed OVX mice. (K) The interacting protein network of SIRT3. (L) Cardiac mitochondrial SOD2 activity in each group. n = 6 for each group, mean ± SEM, $^{*}P < 0.05$ *versus* the sham group, $^{\#}P < 0.05$ *versus* the OVX + HFD group.

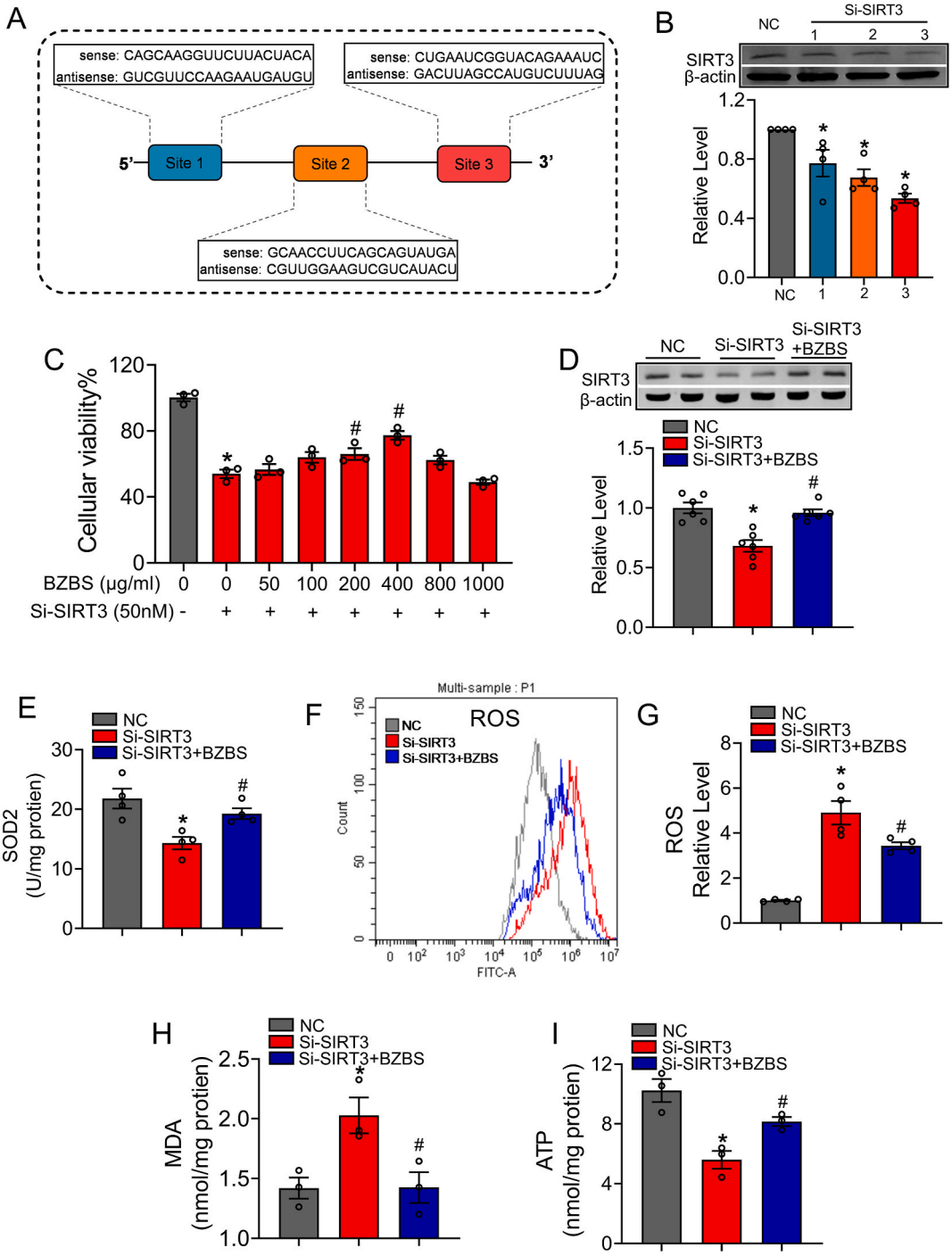

Fig. 6. BZBS regulated the SIRT3/SOD2 pathway *in vitro*. (A) Three different sequences of Si-SIRT3. (B) The knockdown efficiency of three different sequences of Si-SIRT3. (C) Effects of BZBS on the viability of cells transfected with Si-SIRT3. (D) SIRT3 expression after Si-SIRT3 transfection and BZBS treatment in each group. (E) Mitochondrial SOD2 activity in all groups. (F) Representative histograms of the mean fluorescent intensity (MFI) of ROS in the three groups. (G) Quantification of the MFI of ROS in the three groups. (H–I) The MDA content (H) and ATP content (I) were detected in each group. n = 3 for each group, mean ± SEM, $^{*}P < 0.05$ *versus* the NC group, $^{\#}P < 0.05$ *versus* the Si-SIRT3 group.

hearts of wild-type (WT) mice (Fig. 5B), and the expression of SIRT2, SIRT3, SIRT4, SIRT5 and SIRT6 was reduced in the hearts of 16-week-old mice fed a high-fat diet compared with those of normal-food mice (Fig. 5C). However, whether the relatively short-term exposure (12 weeks) of OVX and HFD together can induce abnormal expression of SIRT family members is unknown. Therefore, we evaluated the expression of SIRTs 1–6 and found that only the expression of SIRT3 was significantly lower in the hearts of HFD-fed OVX

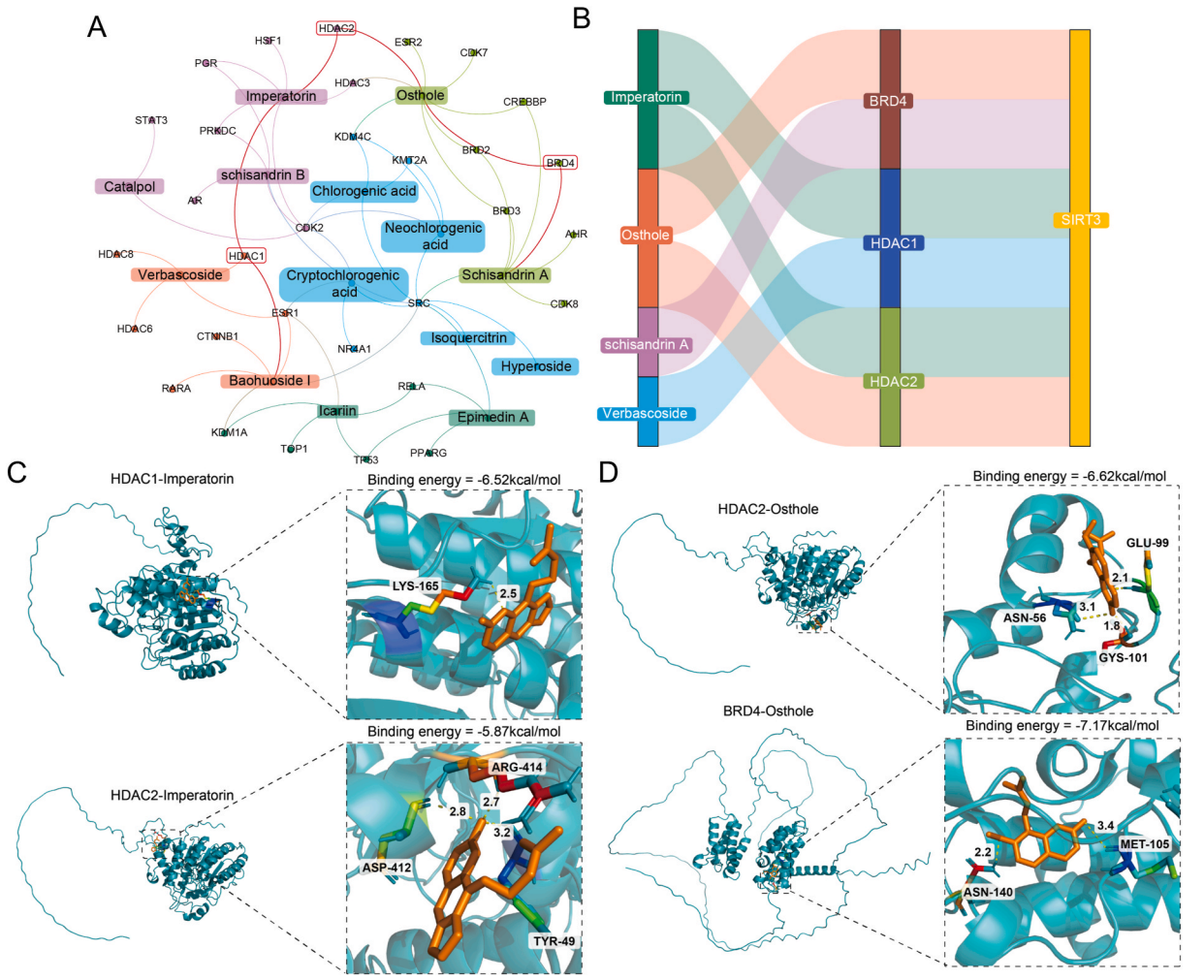

Fig. 7. Ligand interaction and binding diagrams of components in BZBS to transcription factors of SIRT3. (A) The network included 14 components from BZBS and their corresponding targets, which have the potential to act as transcription factors. (B) Relationships between components of BZBS, transcription factors, and SIRT3. (C) The location of imperatorin in the active site of HDAC1 and HDAC2. (D) The location of osthole in the active site of HDAC2 and BRD4. The rainbow structures are referred to as ligands. The yellow dotted line represents hydrogen bonds. The orange structures represent the residues corresponding to HDAC1, HDAC2, and BRD4.

mice than in those of sham control mice; however, the expression of the other 5 SIRTs did not change (Fig. 5D–J). Notably, the reduced SIRT3 protein level in the heart of HFD-fed OVX mice was successfully reversed by BZBS treatment (1.4 and 2.8 g/kg) (Fig. 5D and G), suggesting that BZBS may target SIRT3 to exert its antioxidative stress effect. More importantly, BZBS did not affect the expression of SIRT1, SIRT2, SIRT4, SIRT5, or SIRT6, which remained unchanged in the hearts of HFD-fed OVX mice, indicating that BZBS could improve the reduction in protein expression but did not change the normal protein level (Fig. 5D–J). SIRT3 and downstream signaling are critical for regulating mitochondrial oxidative stress [36]. Then, we used the STRING database to construct the PPI of SIRT3 and its interacting proteins. Through PPI analysis, we found that mitochondrial SOD (SOD2) and NDUFA9 had a high degree of nodes in the SIRT3-interacting protein network (Fig. 5K). SOD2 is a key mitochondrial antioxidant enzyme. SIRT3 impairment reduces the activity of SOD2, which induces mitochondrial ROS accumulation [37]. Activation of the SIRT3/SOD2 pathway could inhibit oxide-induced cardiac hypertrophy in high-fat and high-sucrose diet-fed mice [38]. We then measured the SOD2 activity of cardiac mitochondria in each group. SOD2 activity in cardiac mitochondria in HFD-fed OVX mice was significantly decreased and recovered by treatment with BZBS (1.4 and 2.8 g/kg) (Fig. 5L). These results imply that BZBS can ameliorate the impairment of the cardiac SIRT3/SOD2 pathway in HFD-fed OVX mice.

To further confirm whether BZBS exerts an antioxidative effect via the SIRT3/SOD2 pathway, we transfected small interfering RNAs (siRNAs) (si-SIRT3) into H9C2 cells. To find a more knockdown efficiency Si-RNA, we designed three Si-SIRT3 sequences according to three different mRNA regions in SIRT3 (Fig. 6A). We found that the Si-SIRT3 at site 3 had the best knockout efficiency verified by both qRT-PCR and Western blot test (Fig. 6B and Fig. S2); this sequence was subsequently selected for subsequent experiments. To identify the best dose of BZBS *in vitro*, we transfected Si-SIRT3 into H9C2 cells to induce cytotoxicity by MTT and

observed cell viability after BZBS treatment at different dosages. BZBS improved cell viability at concentrations between 200 μg/mL and 400 μg/mL, and BZBS had the greatest effect on cell survival at 400 μg/mL. Therefore, the concentration of BZBS was set at 400 μg/mL (Fig. 6C). After Si-SIRT3 transfection for 48 h, we found decreased SIRT3 expression (Fig. 6D) and SOD2 activity (Fig. 6E) in H9C2 cells. The combination of BZBS and Si-SIRT3 transfection reversed these reductions (Fig. 6D and E). As expected, inhibiting the SIRT3/SOD2 pathway induced the accumulation of ROS, and BZBS effectively reduced the mitochondrial ROS level in H9C2 cells (Fig. 6F and G). In addition, BZBS reversed the increase in MDA production and decrease in ATP levels in H9C2 cells transfected with Si-SIRT3 (Fig. 6H and I). Collectively, these results indicate that increasing in the activity of the SIRT3/SOD2 pathway involves in the antioxidative effect of BZBS on the hearts of HFD-fed OVX mice.

3.5. Molecular docking of components of BZBS to the transcription factors of SIRT3

Since protein expression levels are mostly regulated by transcription factors, we next screened whether some transcription factors had binding sites for the 14 compounds using hTFtarget. We identified 31 potential transcription factors in BZBS-related targets (Fig. 7A), three of which have binding sites in the promoter region of the SIRT3 gene (Fig. 7B), which were previously reported to regulate SIRT3 expression [39]. The three transcription factors are histone deacetylase 1 (HDAC1), histone deacetylase 2 (HDAC2), and bromodomain-containing protein 4 (BRD4). By tracking the compounds that had to interact with these transcription factors, imperatorin, osthole, schisandrin A, and verbascoside were identified (Fig. 7B). To further identify the possible interactions between these compounds and transcription factors, we downloaded the 3D structures of the 4 screened compounds from NCBI-PubChem for flexible docking studies. Based on common molecular docking criteria, a binding energy ≤ -5 kcal/mol is considered successful docking [40]. We ranked the docking scores (Fig. S3A) and found that imperatorin and osthole were good candidates because the binding energies of imperatorin with HDAC1 and HDAC2 were −6.52 kcal/mol and −5.87 kcal/mol, respectively (Fig. 7C), and the binding energies of osthole with HDAC2 and BRD4 were −6.62 kcal/mol and −7.17 kcal/mol, respectively (Fig. 7D). However, the binding energy of verbascoside with HDAC1 was −1.44 kcal/mol (Fig. S3B), and the binding energy of schisandrin A with BRD4 was −3.73 kcal/mol (Fig. S3C), suggesting weak binding. These results suggest that the binding of imperatorin and ostiole to HDAC1, HDAC2, and BRD4 might be the mechanism by which BZBS regulates the expression of SIRT3.

4. Discussion

BZBS is a Chinese medicine capsule that is clinically used to alleviate aging-related fatigue and forgetfulness. In this study, we highlighted how BZBS has a cardioprotective effect on HFD-fed OVX mice. We observed that the mechanism of BZBS ameliorating cardiac systolic injury in HFD-fed OVX mice is related to the activation of SIRT3/SOD2 pathway. In particular, we found that imperatorin and osthole, which are components of BZBS, might be the key bioactive compounds that play a protective role in the heart function of HFD-fed OVX mice. This work revealed that BZBS is a good candidate drug for preventing or treating cardiac injury in aging or ovariectomized obese females.

Menopause is often associated with aging in women [2]. Preventing and mitigating menopause-related diseases is the key to achieving a healthy aging life for women. Among the many diseases associated with menopause in women, cardiovascular diseases are more common and deadly [41]. Importantly, both clinical and animal studies have shown that a HFD significantly increases the risk of cardiac dysfunction in postmenopausal females [6,8]. Clarifying the molecular pathological features of the heart of menopausal females fed a HFD and developing related effective drugs are crucial for preventing and treating cardiac impairment in aging or ovariectomized obese females. In this study, we first reported that HFD-fed OVX mice displayed cardiac senescence, which was indicated by an increase in the positive β-galactosidase signal and obvious systolic injury without changes in cardiac diastolic function. Importantly, we found that treatment of mice with BZBS successfully prevented cardiac senescence and systolic injury.

To elucidate the molecular mechanism of cardiac systole injury in HFD-fed OVX mice, we initially used bioinformatics methods to identify potentially altered key molecules and found that both heart-specific ER knockout and HFD could induce abnormal expression of the SIRTs family after 16–18 weeks of exposure. In this study, we found that the level of SIRT3, but not the other SIRTs in the family, was significantly reduced in the hearts of OVX mice fed a HFD for 12 weeks. These results suggest that SIRT3 is a more susceptible molecule than the other SIRTs in the family. SIRT3 is located in the mitochondria and regulates SOD2 enzymatic activity to reduce mitochondrial oxidative damage [37]. Interestingly, markedly remodeled mitochondria were also observed in the cardiomyocytes from HFD-fed OVX mice. Importantly, BZBS not only prevented mitochondrial structure damage but also reversed the increase in cardiac ROS and MDA levels and the decrease in ATP levels via the SIRT3/SOD2 pathway in the hearts of HFD-fed OVX mice. These beneficial effects are related to improvements in the activity of the SIRT3/SOD2 pathway. Similarly, the antioxidant effect of BZBS through the SIRT3/SOD2 pathway was also verified *in vitro*. These results suggested that BZBS exerts cardiac antioxidant effects to alleviate systolic damage in HFD-fed OVX mice through the SIRT3/SOD2 pathway.

Dyslipidemia can lead to mitochondrial dysfunction and heart failure [42]. In this study, we found that the cardiomyocytes of HFD-fed OVX mice showed significantly increased lipid droplets. The key point was that BZBS effectively improved blood lipid levels and reduced the number of lipid droplets in cardiomyocytes of HFD-fed OVX mice. These results suggest that the cardioprotective effect of BZBS may also be related to the improved lipid profile. However, how BZBS improves heart function by regulating blood lipids in HFD-fed OVX mice needs further investigation.

The bottleneck in the study of TCM compounds is how to clarify which ingredient is the core ingredient of the drug. Although BZBS contains 16 different ingredients, a previous study reported that 14 main components were detected by UPLC of BZBS [43]. We then explored which of the 14 components is the key compound. Since most of the protein expression was regulated by transcription factors,

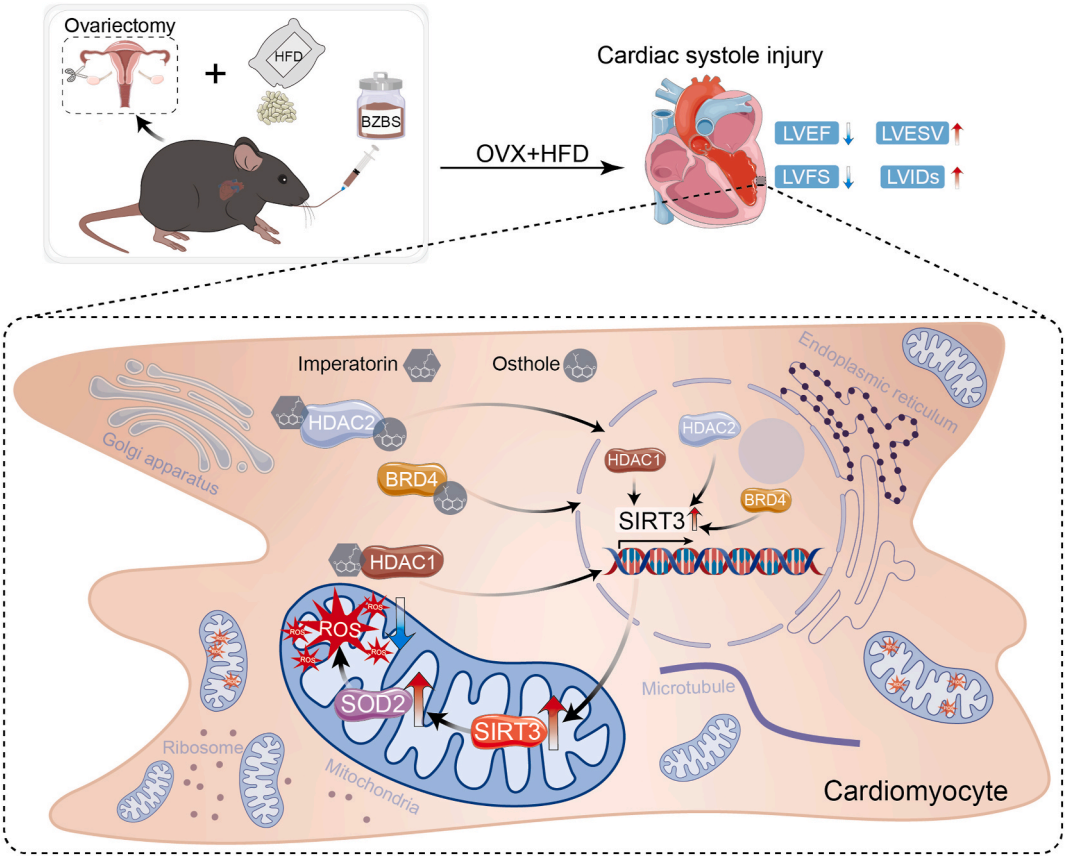

Fig. 8. The mechanism by which BZBS improves cardiac systole injury by targeting SIRT3/SOD2 pathway.

we first screened the potential transcription factors that might interact with the 14 compounds and identified 31 transcription factors. Thereafter, we found that imperatorin or osthole could bind to HDAC1, HDAC2, and BRD4, which were previously reported to be increased in HFD-fed or OVX mice [44–46]. However, whether imperatorin or osthole regulates HDAC1, HDAC2, and BRD4 to rescue cardiac dysfunction by alleviating mitochondrial oxidative damage in HFD-fed estrogen-deficient mice via the targeting of SIRT3 needs to be further studied.

5. Conclusion

Overall, we are the first to report that the activation of SIRT3/SOD2 pathway is an effective way for BZBS to improve cardiac systolic injury of HFD-fed OVX mice and that the compounds imperatorin and osthole in the BZBS may be involved in this process (Fig. 8). This study highlighted the anti-cardiac aging effect of BZBS through the protection of cardiac mitochondria.

Funding statement

This work was supported by the S&T Program of Hebei (No. E2020100001 and NO. 22372502D); the S&T Program of Shijiazhuang (No. 231790133A); the High-level S & T Innovation and Entrepreneurship Talent Project of Shijiazhuang (No. 07202203); the Strategic Consulting Project of the Chinese Academy of Engineering: Strategic research on anti-aging effect of Traditional Chinese Medicine (Grant No. 2022-XY-45); the STI2030-Major Projects (2022ZD0211804); the Key Research and Development Program of Heilongjiang Province (GA21C009 to J. A.); and the Heilongjiang Touyan Innovation Team Program.

Ethical statement

All animal procedures were approved by the Institutional Animal Care and Use Committee at Harbin Medical University (No. IRB3000722) and the Institute of Laboratory Animal Science of China (A5655-01). All procedures conformed to Directive 2010/63/EU of the European Parliament and the ARRIVE guidelines.

Data availability statement

All data included in article/supp. Material/referenced in article.

CRediT authorship contribution statement

Xiaobin An: Writing – review & editing, Writing – original draft, Visualization, Investigation. **Wentao Xu:** Writing – review & editing, Writing – original draft, Investigation. **Xinyue Zhao:** Methodology. **Haihui Chen:** Methodology, Investigation. **Jinan Yang:** Methodology. **Yan Wu:** Investigation. **Dongyang Wang:** Methodology. **Wei Cheng:** Investigation. **Hongrong Li:** Investigation. **Lu Zeng:** Methodology. **Jing Ma:** Investigation. **Qin Wang:** Methodology. **Xuqiao Wang:** Methodology. **Yunlong Hou:** Supervision, Project administration, Funding acquisition. **Jing Ai:** Writing – review & editing, Writing – original draft, Supervision, Project administration, Funding acquisition, Conceptualization.

Declaration of competing interest

The authors declare that they have no known competing financial interests or personal relationships that could have appeared to influence the work reported in this paper.

Acknowledgments

We wish to extend our thanks to any individual for their assistance in the conduction of this study.

Appendix A. Supplementary data

Supplementary data to this article can be found online at https://doi.org/10.1016/j.heliyon.2024.e32159.

References

[1] S.E. Reis, et al., Estrogen is associated with improved survival in aging women with congestive heart failure: analysis of the vesnarinone studies, J. Am. Coll. Cardiol. 36 (2) (2000) 529–533.
[2] S.R. Davis, et al., Menopause, Nat. Rev. Dis. Prim. 1 (2015) 15004.
[3] S.R. El Khoudary, et al., Menopause transition and cardiovascular disease risk: implications for timing of early prevention: a scientific statement from the American heart association, Circulation 142 (25) (2020) e506–e532.
[4] N. Xie, et al., NAD(+) metabolism: pathophysiologic mechanisms and therapeutic potential, Signal Transduct. Targeted Ther. 5 (1) (2020) 227.
[5] M. Ogrodnik, et al., Obesity-induced cellular senescence drives anxiety and impairs neurogenesis, Cell Metabol. 29 (5) (2019) 1061–1077.e8.
[6] M. Soleymani, et al., Dietary patterns and their association with menopausal symptoms: a cross-sectional study, Menopause 26 (4) (2019) 365–372.
[7] M.R. Mouridsen, et al., Modest weight loss in moderately overweight postmenopausal women improves heart rate variability, Eur J Prev Cardiol 20 (4) (2013) 671–677.
[8] K. Shinlapawittayatorn, et al., Sexual dimorphism in cardiometabolic and cardiac mitochondrial function in obese rats following sex hormone deprivation, Nutr. Diabetes 12 (1) (2022) 11.
[9] D. Ali, et al., High-fat diet-induced obesity augments the deleterious effects of estrogen deficiency on bone: evidence from ovariectomized mice, Aging Cell 21 (12) (2022) e13726.
[10] D. Huang, et al., The role of collateral disease theory in the prevention and treatment of atherosclerosis in post-menopausal women: a narrative review, Ann. Palliat. Med. 9 (4) (2020) 2314–2322.
[11] T. Wang, et al., Repositioning of clinically approved drug Bazi Bushen capsule for treatment of Aizheimer's disease using network pharmacology approach and in vitro experimental validation, Heliyon 9 (7) (2023) e17603.
[12] X. Mao, et al., Bazi Bushen mitigates epigenetic aging and extends healthspan in naturally aging mice, Biomed. Pharmacother. 160 (2023) 114384.
[13] L. Li, et al., BaZiBuShen alleviates altered testicular morphology and spermatogenesis and modulates Sirt6/P53 and Sirt6/NF-κB pathways in aging mice induced by D-galactose and NaNO(2), J. Ethnopharmacol. 271 (2021) 113810.
[14] D. Huang, et al., Chinese medicine Bazi Bushen capsule improves lipid metabolism in ovariectomized female ApoE-/- mice, Ann. Palliat. Med. 9 (3) (2020) 1073–1083.
[15] D. Huang, et al., Bazi bushen capsule alleviates post-menopausal atherosclerosis via GPER1-dependent anti-inflammatory and anti-apoptotic effects, Front. Pharmacol. 12 (2021) 658998.
[16] D. Wang, et al., Estrogen-like effect of Bazi bushen capsule in ovariectomized rats, J. Vis. Exp. (2023) 194.
[17] J.A. Amorim, et al., Mitochondrial and metabolic dysfunction in ageing and age-related diseases, Nat. Rev. Endocrinol. 18 (4) (2022) 243–258.
[18] A.E. Kane, D.A. Sinclair, Sirtuins and NAD(+) in the development and treatment of metabolic and cardiovascular diseases, Circ. Res. 123 (7) (2018) 868–885.
[19] B. Schwer, E. Verdin, Conserved metabolic regulatory functions of sirtuins, Cell Metabol. 7 (2) (2008) 104–112.
[20] L. Zhao, et al., MicroRNA-140-5p aggravates doxorubicin-induced cardiotoxicity by promoting myocardial oxidative stress via targeting Nrf 2 and Sirt2, Redox Biol. 15 (2018) 284–296.
[21] S. Song, et al., Sirtuin 3 deficiency exacerbates diabetic cardiomyopathy via necroptosis enhancement and NLRP3 activation, Acta Pharmacol. Sin. 42 (2) (2021) 230–241.
[22] B. Kura, et al., Oxidative stress-responsive MicroRNAs in heart injury, Int. J. Mol. Sci. 21 (1) (2020).
[23] M. Luo, et al., Estrogen deficiency exacerbates learning and memory deficits associated with glucose metabolism disorder in APP/PS1 double transgenic female mice, Genes Dis 9 (5) (2022) 1315–1331.
[24] H. Wu, et al., Deficiency of mitophagy receptor FUNDC1 impairs mitochondrial quality and aggravates dietary-induced obesity and metabolic syndrome, Autophagy 15 (11) (2019) 1882–1898.
[25] L.Y. Sun, et al., MicroRNA-23a mediates mitochondrial compromise in estrogen deficiency-induced concentric remodeling via targeting PGC-1α, J. Mol. Cell. Cardiol. 75 (2014) 1–11.

[26] S. Zhang, et al., AhR/miR-23a-3p/PKCalpha axis contributes to memory deficits in ovariectomized and normal aging female mice, Mol. Ther. Nucleic Acids 24 (2021) 79–91.
[27] D.D. Belke, et al., Insulin signaling coordinately regulates cardiac size, metabolism, and contractile protein isoform expression, J. Clin. Invest. 109 (5) (2002) 629–639.
[28] N. Wang, et al., MicroRNA-23a participates in estrogen deficiency induced gap junction remodeling of rats by targeting GJA1, Int. J. Biol. Sci. 11 (4) (2015) 390–403.
[29] N. El Khoury, S. Mathieu, C. Fiset, Interleukin-1β reduces L-type Ca2+ current through protein kinase Cε activation in mouse heart, J. Biol. Chem. 289 (32) (2014) 21896–21908.
[30] G.L. Xue, et al., Interleukin-17 upregulation participates in the pathogenesis of heart failure in mice via NF-κB-dependent suppression of SERCA2a and Cav 1.2 expression, Acta Pharmacol. Sin. 42 (11) (2021) 1780–1789.
[31] C. Ji, et al., Bazi Bushen capsule attenuates cognitive deficits by inhibiting microglia activation and cellular senescence, Pharm. Biol. 60 (1) (2022) 2025–2039.
[32] M.A. Aon, N. Bhatt, S.C. Cortassa, Mitochondrial and cellular mechanisms for managing lipid excess, Front. Physiol. 5 (2014) 282.
[33] M.Y. Liu, et al., TIGAR drives colorectal cancer ferroptosis resistance through ROS/AMPK/SCD1 pathway, Free Radic. Biol. Med. 182 (2022) 219–231.
[34] Z. Zhu, et al., Negative effects of ROS generated during linear sperm motility on gene expression and ATP generation in boar sperm mitochondria, Free Radic. Biol. Med. 141 (2019) 159–171.
[35] P.I. Merksamer, et al., The sirtuins, oxidative stress and aging: an emerging link, Aging (Albany NY) 5 (3) (2013) 144–150.
[36] X. Liu, et al., Sirt3-dependent regulation of mitochondrial oxidative stress and apoptosis contributes to the dysfunction of pancreatic islets after severe burns, Free Radic. Biol. Med. 198 (2023) 59–67.
[37] A.E. Dikalova, et al., Sirt3 impairment and SOD2 hyperacetylation in vascular oxidative stress and hypertension, Circ. Res. 121 (5) (2017) 564–574.
[38] U.J. Yun, D.K. Yang, Sinapic acid inhibits cardiac hypertrophy via activation of mitochondrial sirt3/SOD2 signaling in neonatal rat cardiomyocytes, Antioxidants 9 (11) (2020).
[39] Q. Zhang, et al., hTFtarget: a comprehensive database for regulations of human transcription factors and their targets, Dev. Reprod. Biol. 18 (2) (2020) 120–128.
[40] Y. Feng, et al., Yindan Jiedu granules exhibit anti-inflammatory effect in patients with novel Coronavirus disease (COVID-19) by suppressing the NF-κB signaling pathway, Phytomedicine 95 (2022) 153784.
[41] L. Newson, Menopause and cardiovascular disease, Post Reprod. Health 24 (1) (2018) 44–49.
[42] L. Da Dalt, et al., Cardiac lipid metabolism, mitochondrial function, and heart failure, Cardiovasc. Res. 119 (10) (2023) 1905–1914.
[43] Q. Liu, et al., Sirtuin 3 protects against anesthesia/surgery-induced cognitive decline in aged mice by suppressing hippocampal neuroinflammation, J. Neuroinflammation 18 (1) (2021) 41.
[44] C. Hu, et al., HDAC1 and 2 regulate endothelial VCAM-1 expression and atherogenesis by suppressing methylation of the GATA6 promoter, Theranostics 11 (11) (2021) 5605–5619.
[45] J. Mu, et al., BRD4 inhibition by JQ1 prevents high-fat diet-induced diabetic cardiomyopathy by activating PINK1/Parkin-mediated mitophagy in vivo, J. Mol. Cell. Cardiol. 149 (2020) 1–14.
[46] Y. Liu, et al., A novel BRD4 inhibitor suppresses osteoclastogenesis and ovariectomized osteoporosis by blocking RANKL-mediated MAPK and NF-κB pathways, Cell Death Dis. 12 (7) (2021) 654.